INFLUENCE OF DYNAMIC FLAP MOVEMENT ON MAXIMUM LIFT AND WAKE VORTEX EVOLUTION

R. Stephan, M. Bremm, R. Hörnschemeyer, E. Stumpf
Institute of Aerospace Systems, RWTH Aachen
Wüllnerstr. 7, 52062 Aachen, Germany

H. Schmidt, K.-U. Schröder
Institute of Structural Mechanics and Lightweight Design, RWTH Aachen
Wüllnerstr. 7, 52062 Aachen, Germany

J. Ruhland, C. Breitsamter
Chair of Aerodynamics and Fluid Mechanics, Technical University of Munich
Boltzmannstr. 15, 85748 Garching bei München, Germany

Abstract

For low drag and low complexity reasons, the use of enforced instationary aerodynamic phenomena has not been exploited on large aircraft so far. Modern fly-by-wire aircrafts with e.g. Advanced Dropped Hinged Flaps generally offer the architecture in which a periodical oscillation of the flaps is possible when an adapted actuator concept is applied. Either, this capability can be used for a periodic alteration of the spanwise lift distribution and with it the wake vortex centroid positions in order to accelerate exponential growth of natural vortex wake instabilities for fast vortex wake decay. Or, the constant periodic oscillation of flaps allows for higher deflection angles and respectively larger maximum lift coefficients compared to classical high-lift conditions with constant flap deflection angles due to the dynamic lift effect. Motivation of the former concept is a potential reduction of separation distances during approach whereas the latter concept might contribute to reducing airplane weight and exhaust fume emission or enable alternative approach trajectories. Within the research project BIMOD, funded by the German Aeronautic Research Program LuFo V-3, RWTH Aachen University and TU Munich cooperate on investigating the two concepts on a fundamental basis and on exploring the design space for respective technology implementation into current airliners. Preliminary results have shown that at a reduced frequency scope around 0.08 ± 0.01 the wake vortex instability is excited, while the dynamic high-lift enhancement is largely dependent on the flap gap and kinematics.

Keywords

Wake vortex instabilities, lift coefficient, experimental, high-lift design, structural design

1. INTRODUCTION

A dynamic change of lift distribution is known to have the potential to alter the wake vortex development as well as the maximum achievable lift.

By introducing frequencies corresponding to natural instabilities of the wake vortex system, an accelerated decay of the vortices can be triggered and thus, the hazard to following aircraft and related airport capacity constraints imposed by vortex wakes can be reduced. In BIMOD, this periodic change of spanwise lift distribution is realized by counter-acting oscillation of trailing edge flaps.

Given the oscillation of flaps a second phenomenon, namely the dynamic lift potential caused by hysteresis effects, can be furthermore exploited. By periodic oscillation of the flaps, separation is delayed thus higher deflection angles can be realized. Consequently, an increased maximum overall lift is achievable.

The research project BIMOD aims on investigating the two potential applications of oscillating flaps described above.

doi:10.25967/490118

Review wake vortex instability excitation

Several reviews provide information on past and present research in the field of wake vortex systems [8], [12], [18], [28], [33]. The studies present fundamental physical investigations with regard to modelling, instabilities and transient flow. Other studies deal with developments and applications of methods deriving from experimental and numerical simulation for the representation and analysis of all development stages of a wake vortex system. A further focus of the investigations is the simulation and prediction of the behaviour and decay of wake vortex system in the atmosphere as well as the development and testing of detection and wake vortex warning systems. In the seventies, extensive model studies and flight tests were carried out in connection with the determination of the separation distances [4], [5], [15], [16], [22], [29]. In view of the importance of the wake vortex problem for the European aviation industry, various research projects and joint research programmes with the topics vortex prediction, detection and consideration as well as vortex strength reduction were initiated [12], [17], [20], [21].
In this paper, the reduction of the wake vortex system by means of oscillating flaps is investigated.

Review high-lift regarding oscillating airfoils

Efforts to increase the lift or the lift coefficient are the subject of research for a long time. Early studies on the influence of boundary layer separation, lift increase and flow excitation measures were carried out [1], [7]. Most studies investigate dynamic loads on a wing oscillating around the pitch axis.
The possibility of influencing the total lift by an oscillation of the angle of attack was also recognized. Starting in the early 1990s, investigations with an oscillation around the pitch axis were presented for delta wings, which describe the hysteresis effect for the lift coefficient in great detail [3], [23]. GREENBLATT and WYGNANSKI [13] give an overview of the work of the last century in this field. In 1999 GREENHALGH [14] was granted a patent for oscillating flaps to increase lift. This patent uses a very generic model to show the results of investigations in which the lift coefficient is increased with increasing oscillation frequency. Recently, a study has examined the oscillatory actuation of the trailing edge flap as a potential mechanism to increase the lift coefficient [32].
Despite the early findings that oscillating rudder surfaces can lead to an increase in the maximum lift coefficient and a patent on this, hardly any studies consider the potential for civil aviation. Experimental and numerical investigations are mainly carried out on very simplified models and are mostly aimed at rotor blades as an application. In particular, no studies are known that consider this aspect in the entire airplane, taking into account all systems and structural requirements.

This paper investigates both the influence of oscillating flaps on the wake vortex instabilities and on the maximum lift. In addition, investigations regarding the transfer to the overall airplane level with regard to high-lift and structure design are considered.

In order to investigate these two different effects, an airplane configuration is set up as a baseline model. An aerodynamic preliminary design analysis of the configuration is conducted by means of computational fluid dynamics. Based on the results of the aerodynamic analysis, high-lift devices are integrated as Advanced Dropped Hinge Flaps in the configuration.

To investigate the influence on wake vortex evolution, numerical investigations are made with respect to the excitation of wake vortex instabilities by means of oscillating flaps. Using these results, a model referring to the airplane configuration for wind tunnel experiments to examine the influence of wake vortex system has been manufactured and studied.

Subsequently, the influence on the maximum lift coefficient by dynamically deflecting flaps and exploiting the hysteresis effect is being investigated. A simplified wing model with a periodic oscillating plain flap has been designed for investigations in a water tunnel to determine the lift forces at different oscillation frequencies and to investigate the interaction of oscillation frequencies, amplitudes and lift.

Based on the oscillation frequencies of the flap determined for wake vortex and high lift influence, a design of actuator allocation and structure is conducted.

2. AIRPLANE CONFIGURATION

In this chapter, the airplane configuration is described, on which basis the further steps of processing are carried out. Subsequently, the architecture and geometry of the high-lift system are defined.

2.1. Airplane configuration

A long-range airplane, hereinafter referred to as LR-270, with a maximum take-off mass (MTOM) of 270 t is designed with the aircraft design software MICADO [27] of the Institute of Aerospace Systems. For the calculation various semi-empirical methods such as described by TORENBEEK [35], RAYMER [24] and HOWE [19] are used together with analytical tools in order to carry out the entire airplane preliminary design under specification of a few top-level airplane requirements (TLARs) and design constraints. A picture of the designed airplane can be found in the appendix in figure A.1. The LR-270 is specifically chosen because it is close to a real airplane that uses Advanced Dropped Hinge Flaps as a trailing edge flap system.

The data of the LR-270 are shown in table 1. The corresponding flight envelope is shown in figure 1.

2.2. High-lift system architecture

Since fast flap deflections are to be provided for the system design, there are three main requirements. Firstly (a) the achievable $\Delta c_{l,\max}$ is important, secondly (b) the system

MASS		
Maximum Takeoff Mass (MTOM)	270000	kg
Operating Mass Empty (OME)	135000	kg
Minimum Flight Mass (MFM)	153009	kg
Design Payload	53400	kg
Maximum Fuel Capacity	108328	kg
Engine Mass	8600	kg
Main Landing Gear Mass	4100	kg
GEOMETRY		
Wing half span ($b/2$)	30.5	m
Reference Wing Area (S_{ref})	436.21	m^2
Root Chord (c_{root})	13.47	m
Mean Aerodynamic Chord (MAC)	8.84	m
Kink position from centre (y_{kink})	10.50	m
Aspect Ratio (Λ)	8.53	–
DESIGN DATA		
PAX	325	–
Approach speed	70	m/s
Cruise speed	252	m/s
Design Range	8100	NM

Tab. 1: Mass, geometry and design data of the airplane configuration LR-270.

has to be lightweight and thirdly (c) a low mechanical complexity is desirable.
The Advanced Dropped Hinge Flaps (ADHF) are a high-lift system, which already meets these requirements according to the current state of the art.

(a) A high $\Delta c_{l,\max}$ is achieved by actuated spoilers for gap control [25].

(b) With the increase of the aerodynamic efficiency, smaller and lighter flap systems can be built.

(c) The demand for lower mechanical complexity of the system is derived by the fact, that all components involved in the oscillation movement are exposed to increased wear. The desired lower mechanical complexity [26], [34] is, however, to be seen in relation to other architectures [30], as in the case of swept wings in particular, arrangements must be made for streamwise flap motion [36].

2.3. High-lift geometry

With the base airplane configuration described in chapter 2.1, aerodynamic investigations were carried out by means of numerical simulations. The calculations have been conducted with ANSYS FLUENT. The flow conditions correspond to real landing approach conditions of a transport airplane configuration at $Re = 0.415 \cdot 10^8$, $Ma = 0.21$ and $\alpha = 8°$. The calculated lift coefficients for different flap settings are shown in figure 2.

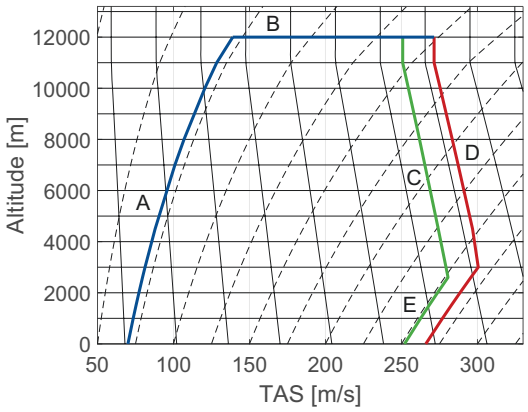

Fig. 1: Flight envelope limitations. A: Stall, B: Altitude, C: Maximum operating speed, D: Dive speed, E: Dynamic pressure.

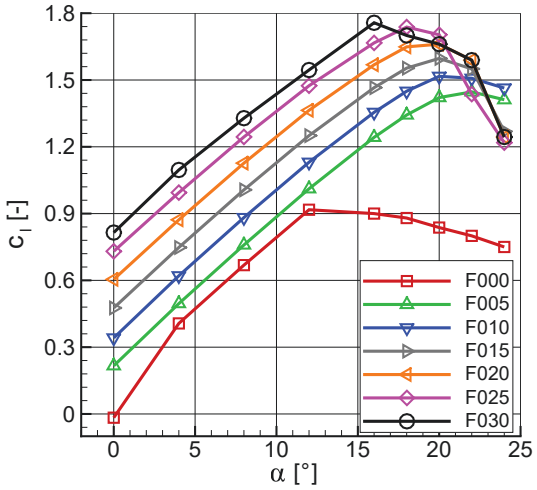

Fig. 2: Calculated lift coefficients for different flap settings at $Re = 0.415 \cdot 10^8$ and $Ma = 0.21$.

On the basis of the calculated aerodynamic forces and moments and further literature research regarding high-lift systems [25], [34], high-lift devices have been integrated into the LR-270 configuration. The respectively chord lengths are listed in table 2. As discussed in chapter 2.2, Advanced Dropped Hinge Flaps, as shown in figure 3, are integrated additionally together with droop nose as leading edge devices, which are not further discussed in this paper.

One of the investigated flap systems is a design of two smaller oscillating outboard flaps (1 and 2) and one conventionally extending inboard flap, with two actuator stations per flap as shown in figure 4.

This is intended to compensate for a non-controllable flap in a failure event. In addition, the two oscillating flaps are designed to produce the same lift. With a counter-rotating oscillation of the flaps lift fluctuations are compensated. The positioning of the oscillating flaps outboard is based on the hypothesis, that a more closely spacing to the centre of vorticity of the wake vortex is able to influence wake vortex more effectively. The geometric dimensions of the conven-

	Flaps	Droop Nose	Spoiler
Mean chord length (related to c_{local})	0.19	0.1	0.25

Tab. 2: Mean chord length of the flap, droop nose and spoiler, related to local wing section chord.

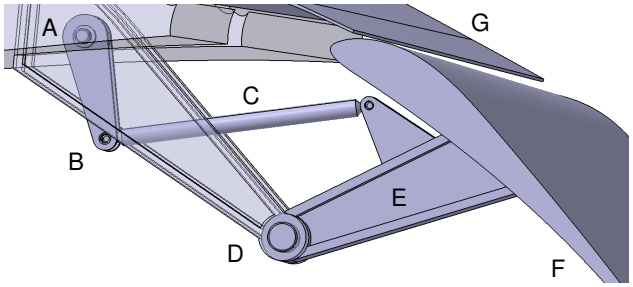

Fig. 3: One actuator station of the implemented Advanced Dropped Hinge Flap with adjusted spoiler. A: Main actuator, B: Link, C: Strut, D: Dropped Hinge, E: Flap spar, F: Flap, G: Actuated spoiler.

tionally extending inboard flap and the two oscillating outboard flaps are shown in table 3. The design of other flap distributions is planned.

Location	Span [m]	Chord inboard [m]	Chord outboard [m]
Inboard	7.50	1.48	1.48
Outboard 1	4.50	1.48	1.20
Outboard 2	5.10	1.20	0.90

Tab. 3: Geometric data of the trailing edge flaps.

On the basis of this airplane configuration and the selected high-lift system, the following chapters examine the wake vortex, the lift coefficient and a more detailed high-lift and structural design.

3. DECREASING THE SEPARATION DISTANCES BETWEEN AIRPLANES BY EXCITATION OF WAKE VORTEX INSTABILITIES

The technical objective is to prove the destabilization of the wake vortex system by periodic excitation using oscillating flaps. For this purpose, the time-dependent velocity fields are measured on a generic airplane model in a wind tunnel. The excitation frequencies regarding the dynamic lift generation as well as the destabilization of the wake vortex system have to be coordinated. Furthermore, the farfield of the wake vortex system is investigated complementarily numerically by means of a LES approach. The conditioning of the LES takes place by experimental data as well as time-resolved Navier-Stokes calculations (Unsteady

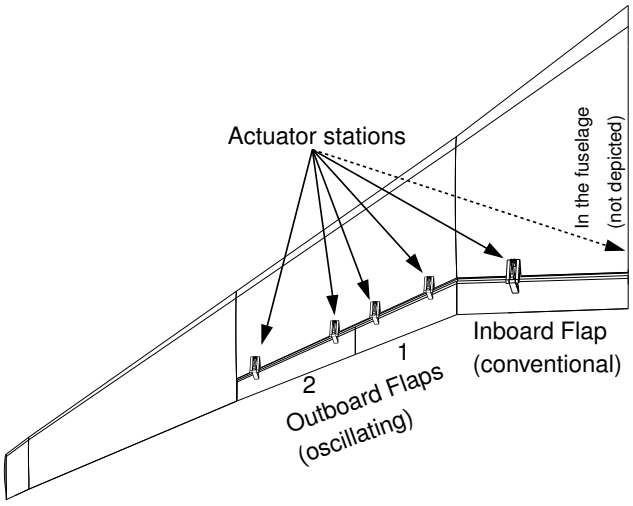

Fig. 4: Flap system design and actuator station distribution.

Reynolds Averaged Navier-Stokes - URANS). This results in a detailed database for the evaluation of the flow-field characteristics. Finally, models of reduced order (ROM) are developed.

3.1. Theoretical background for the investigated vortex instabilities

The most significant long-wave instability for a vortex pair is the Crow instability [2], [6]. This instability is caused by mutual induction and the sinusoidal deformation is the result of instability growing after initial disturbances like airplane wake turbulence and atmospheric turbulence. The inclination of the perturbation plane is given by

$$\Theta = \arccos\left(\pm\sqrt{\frac{-\Gamma_2}{2\cdot\Gamma_1}}\right). \tag{1}$$

For a vortex pair with the same circulation, the sinusoidal deflection is formed in planes with an angle of approximately 45° to the horizontal. The deflection amplitude grows exponentially over time, but the gain factor is low. Due to the deflection, the two vortices come into contact and the circulation or vorticity of the opposite sign is exchanged across the plane of symmetry. As a result, the vortex filaments break up and vortex rings are formed which quickly disintegrate into smaller structures and finally dissipate. This type of instability is ultimately responsible for the disintegration of the wake vortex system in the farfield. With oscillating trailing edge flaps, a disturbance in the flow is now to be induced in the near field. In this way, the collapse of the wake vortex system is to be triggered at a much earlier point in time. The characteristic wavelength of long-wave instabilities is given by [2], [6]

$$\frac{\lambda_{\mathrm{crow}}}{b_0} = 9.0 \pm 1.0. \tag{2}$$

By means of the definition of reduced frequency k_{crow}

$$k_{\mathrm{crow}} = \frac{f\cdot(b/2)}{U_\infty} = \frac{b}{2\cdot\lambda_{\mathrm{crow}}} \tag{3}$$

and a typical value for b_0 in the range of $b_0 = 0.76 - 0.78\,b$ for today's transport airplanes, a reduced frequency for Crow k_{crow} instability is found

$$k_{\mathrm{crow}} = 0.08 \pm 0.01. \tag{4}$$

Referring to the LR-270 airplane configuration, with a half span of 30.5 m and an approach velocity of 70 m/s, which is examined in this paper and presented in chapter 2.1, the frequency range is $f = 0.161 - 0.207\,\mathrm{Hz}$.

3.2. Numerical and experimental approach

To calculate the forces and moments of the configurations and the nearfield of the wake vortex system, Unsteady Reynolds Averaged Navier Stokes equations (URANS) are solved by means of ANSYS Fluent. For the mid- and farfield Large Eddy Simulations (LES) are done. The LES boundaries are initialized by the results of URANS simulations and experimental data. To model the motion of the flaps, User Defined Functions (UDFs) and Dynamic Mesh methods of ANSYS Fluent are used. For the design of the wind tunnel model, numerical simulations with Mach numbers $Ma = 0.074 - 0.210$ and Reynolds numbers $Re = 0.5 \cdot 10^6 - 41.5 \cdot 10^6$, including the wind tunnel conditions were carried out.

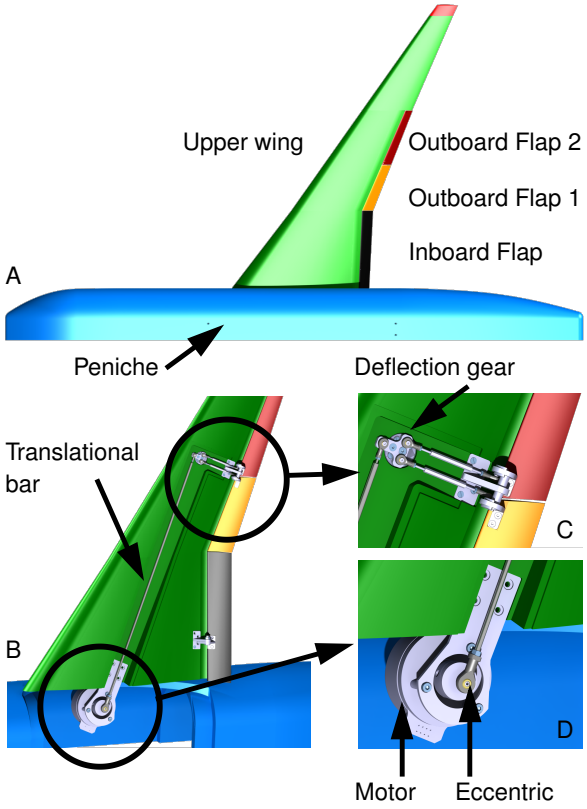

Fig. 5: A: Plan view of wind tunnel model, B: Bottom side of wing without cover, C: Detailed view of deflection mechanism and actuating rods, D: Detailed view of motor, eccentric and translation rod.

Based on CFD data, the deflection angles of the high-lift devices of the wind tunnel model were determined. A droop nose with a deflection angle of DN = 25° was defined over the entire wing span. The spoiler deflection angle for the selected ADHF configuration is fixed at S=6.8° towards the flap. The deflection angle of the trailing edge flap has been set to $\eta = 25°$ for baseline configuration. The flap deflection angle is adjustable in a range from 20° up to 40°. The outboard flaps can oscillate independently from each other around the hinge axis with a maximum amplitude of ±5°. The frequencies are adjustable in a range up to 10 Hz. Investigations with regard to strength and eigenmodes of the model were carried out by means of the software ANSYS Structural Analysis and CATIA V5. The wind tunnel model was designed and manufactured as a half model in a scale of 1:27. The shortened fuselage geometry with integrated peniche, which reduces the influence of the wind tunnel boundary layer on the model, was designed by numerical simulation. The aim was to ensure that no flow separation on the upper side of the fuselage at high angles of attack occurs. A schematic of the model with the divided flaps and actuators is shown in figure 5.

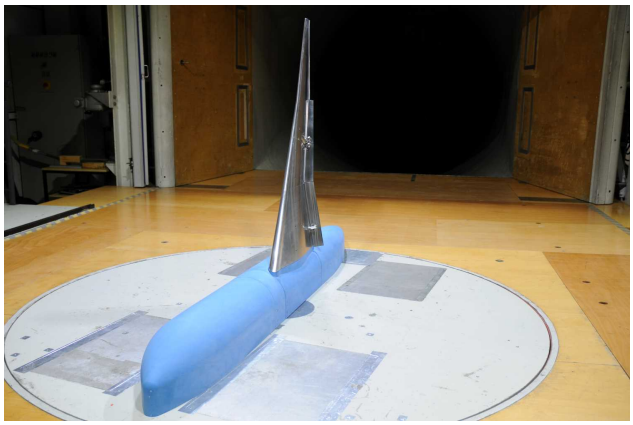

Fig. 6: LR-270 wind tunnel model ($\alpha = 12°$, $\eta = 25°$) in wind tunnel A for force, moment and PIV measurements.

Fig. 7: LR-270 wind tunnel model ($\alpha = 12°$, $\eta = 25°$) in wind tunnel C for hot wire measurements.

Measurements of forces and moments are done in wind tunnel A as shown in figure 6 by means of a six component scale. Furthermore, Particle Image Velocimetry (PIV)

measurements are conducted in wind tunnel A. In wind tunnel C as depicted in figure 7, hot-wire anemometry measurements are performed to capture the vorticity of the wake vortex system in the midfield. Specifications of the wind tunnels A/C of the chair of Aerodynamics and Fluid Mechanics of the TU Munich are listed in the appendix.

3.3. Results

In this chapter, selected results of the hot wire measurements are presented. In order to evaluate the instabilities that occur in the vortex system, characteristic spectral peaks are looked for. These indicate that turbulent kinetic energy is channeled in a narrow band due to quasi-periodic fluctuations. The trailing edge outboard flaps are actuated with a phase shift of 180° at a frequency of $f = 1.8\,\mathrm{Hz}$ ($k_{\mathrm{crow}} = 0.08$). Figure 8 shows the normalized spectral power density $S_{u'}^{N}$ above the reduced frequency k_{crow} for a measuring point at the plane $X^* = 0.06$ ($X^* = X/b$) and for a measuring point at the plane $X^* = 6$. Both points were chosen in the area of the dominant outboard flap vortex. Strong spectral peaks at the introduced frequency $k_{\mathrm{crow}} = 0.08$ are visible for the measurement at $X^* = 0.06$ as well as for the measurement at $X^* = 6$.
Thus, the introduced frequency is propagated downstream of the flow field and the necessary condition for an accelerated wake vortex decay is fulfilled.

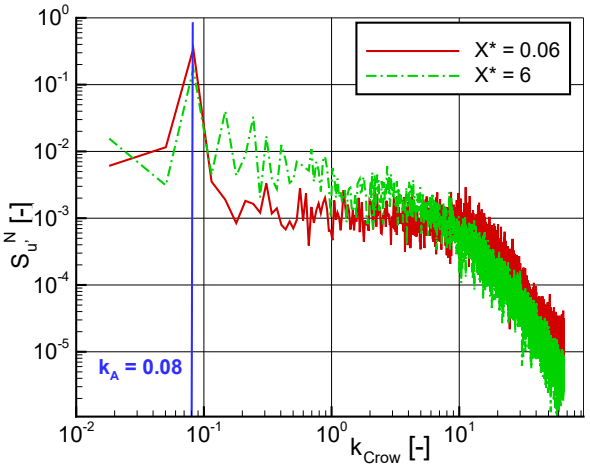

Fig. 8: Normalized spectral power density $S_{u'}^{N}$ as a function of the reduced frequency k_{crow} for measuring points at $X^* = 0.06$ and $X^* = 6$ with $k_{\mathrm{crow}} = 0.08$, $\alpha = 12°$, $U_{\mathrm{ref}} = 25m/s$, $\eta = 25°$, $d\eta = 5°$.

4. INCREASING THE LIFT COEFFICIENT TOWARDS SMALLER AND LIGHTER HIGH-LIFT SYSTEMS

In this chapter, the expected effect of increasing the maximum lift by oscillating flaps is described, together with the experimental setup.

4.1. Theoretical background for increasing lift with oscillating flaps

Various studies indicate that improvements in the lift coefficient can be achieved on a wing when flaps are moved in an oscillating motion. GREENHALGH [14] for example has described the separation of flow at high flap deflections can be prevented by their oscillation. In consequence, higher maximum flap angles respectively larger maximum lift coefficient can be achieved thus a lighter high-lift system structure is allowed.
SHEHATA, ZAKARIA, HUSSEIN, and HAJJ [32] carried out experiments on a rectangular wing with a NACA 0012 profile and a Reynolds number of $Re = 0.21 \cdot 10^5$. Introducing the reduced frequency k as

$$k = \frac{2\pi c f}{U_\infty}, \tag{5}$$

it was concluded that dynamic flap effects has been observed for $k > 0.1$.

In the following, a setup is presented for further investigation of the influence of an oscillating flap at reduced frequencies $k > 0.1$, whereby in this context the influence of other parameters is investigated as well.

4.2. Experimental approach

A wing model was constructed for application in the closed circulating water tunnel to investigate the influence of oscillating trailing edge flaps on the lift coefficient. The focus thereby lies on a generic investigation of two-dimensional flow. Planar particle image velocimetry (PIV) is used to investigate the flow field of a wing with an oscillating flap. The wing consists of a NACA 2412 airfoil with a chord length of $c = 150\,\mathrm{mm}$ and a plain flap at $x/c = 0.8$. Figure 9 shows the nomenclature of the profile. The first rod in the direction of flow fixes the wing at $x/c = 0.25$. The angle of attack can be adjusted via the second rod. The rearmost rod is connected to the flap and allows both the positioning of the flap angle and the periodically oscillating movement around this flap angle by means of an electric motor. The amplitude and frequency of the flap oscillation are variably adjustable.

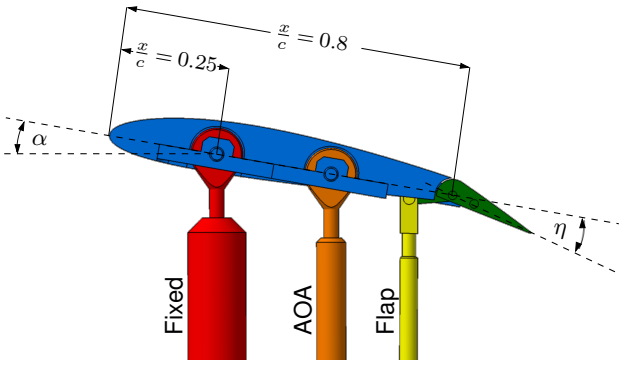

Fig. 9: Nomenclature of the used NACA 2412 airfoil with a chord length of $c = 150\,\mathrm{mm}$ and a plain flap at $x/c = 0.8$.

The wing model is mounted upside down in the measuring section of the enclosed circulating water tunnel as shown

in figure 10. The test section has a length of 1200 mm and a cross section of 540 mm x 540 mm. During the measurements, the water temperature changes due to friction, which has an influence on the Reynolds number. In order to keep the Reynolds number constant, the free stream velocity U_∞ is adjusted accordingly.

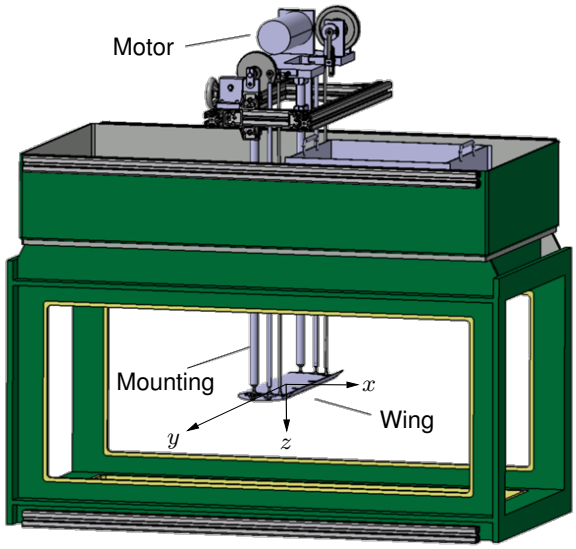

Fig. 10: CAD model of the experimental set-up with the wing mounted upside down spanning the test section. The test section is equipped with glas windows at the bottom and at the top for the laser illumination and on the side for the use of cameras.

For the measurements, two synchronized PIV systems with a total of four cameras and two double pulse lasers are used. PIV measurements are carried out around the entire wing profile within an xz-plane.
The two synchronised double pulse lasers illuminate the lower and the upper side of the wing. The particle reflections are recorded on each wing side with two cameras each, so that the Field of View (FOV) includes the entire wing profile. The cameras are arranged perpendicular to the main flow direction. Within post-processing, a Field of Interest (FOI) is merged from the FOV which contains the complete wing profile as well as the profile flow around it. The obtained information are used to determine the velocity vectors in the FOI that are required for further investigation.

For further evaluation, the circulation is determined from the velocity vectors. It must be ensured that the different flap positions are represented equally frequently in the recorded images during the oscillating flap movement. This can be achieved, for example, by means of correspondingly high recording frequencies of the PIV-measurements and with the use of a rotary encoder for exact determination of the flap position. Table 4 lists the parameters of the planned experiments.

Preliminary results show for an evaluated gapless plain flap a limited influence from the oscillatory movement. In the upcoming experiments, a configuration with a gap and a different kinematics will be evaluated. As RUHLAND and BREITSAMTER [31] have shown, the gap and kinematics design take a strong influence on the lift alternation, whereby a configuration was presented, which shows promising results for $k > 0.2$.

Parameter	Range
Reynolds number (Re)	$Re = 0.21 \cdot 10^5 - 0.30 \cdot 10^6$
Angle of attack (α)	$0° - 15°$
Flap deflaction angle (η)	$0° - 25°$
Reduced frequency (k)	$0 - 2.0$
Oscillation amplitude ($\Delta\delta$)	$5°$

Tab. 4: Parameters of the planned high-lift experiments.

5. FLAP AND STRUCTURAL DESIGN

In this chapter, studies are conducted taking into account the flap design and the structural requirements that are necessary to transfer the results of the previous chapters to the airplane configuration LR-270. Thus in chapter 5.1 a preliminary design of the flaps with regard to mass is carried out. The chapter 5.2 examines the structural requirements and how the oscillation affects the structure.

5.1. Flap and actuator distribution design

Since the mechanical power, which is to be provided by the actuator depends largely on the kinematics of the system and the demanded oscillation characteristics, those conditions have to be defined. Possibilities are mentioned for introducing oscillation into the system by local actuators.

The extension process is derived from the results of the previous chapters. During the extension process, the spoiler is constantly moved up to keep the gap below 2% of the local wing chord [30].
The inboard flap moves to a position of 25° within 30 s. The outboard flaps 1 and 2 move as well to 25° within 30 s, then starting the oscillation around this angle with an amplitude of ±5°. The oscillating attributes derive from the investigations regarding the vortex instabilities (0.207 Hz). In order to achieve this extension behaviour, the following placement of actuators is proposed with particular respect to local actuators.
The depicted system in figure 3 is used for the conventionally extending inboard flap and utilizes a rotary actuator in point A, which is called *main actuator* hereafter. The main actuator provides the conventional flap extension in the first 30 s.
Regarding the oscillating flaps outboard 1 and 2, in addition to the main actuator, the link (B) in figure 3 is equipped with a second actuator, which is referred to as *oscillation actuator* hereafter. This can be either a linear or a rotary actuator to provide the oscillating motion.
The potential types of the actuators are electro-mechanical actuators (EMA) and electro-hydraulic actuators (EHA). The proposed actuators are summed up in table 5.

Location	Movement pattern	Type
Main actuator	Rotary	EMA
Oscillation actuator	Rotary/Linear	EMA/EHA

Tab. 5: Proposed main and oscillation actuators.

In order to dimension the actuators in the next step, some more information about the flap has to be added.
Thus the dimensions of the components shown in figure 3 are relevant, since the aerodynamic forces applied to the flaps are transmitted to the actuators depending on these dimensions.
Additionally, since the outboard flaps oscillate rapidly around the angle of 25°±5°, the moment of inertia I and the angular acceleration $\dot{\omega}$ of the rotating components are important. The resulting additional torque has to be coped with by the actuators. As shown in equation 6, the mass m and the distance r in square from centre of rotation to centre of mass are taken into account [9].

$$M = \frac{dL}{dt} = \frac{d(r^2\, m\, \omega)}{dt} = \dot{\omega}\, I \tag{6}$$

The specifications are summarized in table 6.
The flap mass is determined by the assumption of a CFRP material for the skin and additional 30% of structure weight. Therefore, the flap mass directly scales with the flap area.
The flap spar mass derives from a constructed structural model with titanium as material.

Specifications	Outboard flap 2	Outboard flap 1	Inboard flap
Stations per flap [−]	2	2	2
Actuators per station [−]	1 Main + 1 Oscillating	1 Main + 1 Oscillating	1 Main
Flap mass [kg]	114.7	117.6	216.5
Flap spar mass [kg]	36.2	36.2	42.2
Oscillation frequency [Hz]	0.207	0.207	–
Flap angle [°]	25±5	25±5	25

Tab. 6: Specifications for the actuator stations.

5.2. Structural design

Based on the certification specification for large aircraft CS-25, the wing structure is designed with regard to the deformations and stresses of the wing at the 2.5g manoeuvre. Therein, the design parameter of the structure is the root bending moment. Subsequently, the structure is dimensioned on the basis of the modified flap concept.

5.2.1 Load definition

The structural requirements result from the operational conditions of the flight envelope such as airspeed and altitude as well as requirements resulting from the CS-25 [10] certification requirements.
The geometric and operational boundary conditions of the airplane configuration are based on the airplane configuration data from chapter 2.1. The design weight of the LR-270 configuration is given in table 1. Here the minimum flight weight (MFM) of the LR-270 configuration is based on the Operating Mass Empty (OME) plus a fuel reserve for 45 min flight time according to § 25.343 [10]. The calculation of the quasi-stationary loads is based on the geometric values of the table 1.
The V-n diagram in figure 11 for manoeuvres, represented by a black line, corresponds to the specific requirements of the CS-25 approval regulations, where the maximum positive load factor is limited to 2.5g and −1g for the negative load. The envelope is limited for the low airplane velocities by the stalling speed, dependant on the maximum lift coefficient and the diving speed $v_D = 266\,\mathrm{m/s}$ at $Ma = 0.92$. Based on the modified flap concept the main focus is on the lower flight region of an equivalent airspeed between $EAS = 65 - 80\,\mathrm{m/s}$. Furthermore, the quasi-stationary loads due to gusts can be estimated using the Pratt method [11]. The calculation method is based on the assumption of a rigid airplane.

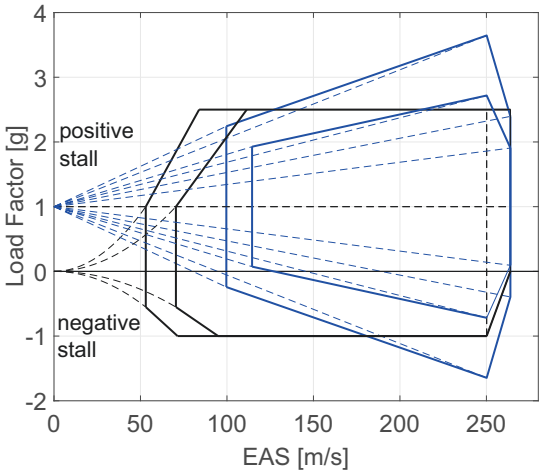

Fig. 11: V-n Diagram of the LR-270 configuration.

5.2.2 Structural wing concept

Based on the data from chapter 2, a parametric wing model was first developed for the preliminary design. The reference wing is modelled as a classical wingbox with front- and rearspar, rips and stringer stiffened shell elements. The frontspar is placed at 20% wing chord length and the

rearspar is placed at 60% wing chord length. The stringers has been modelled by a smeared stiffness of the shell elements. The centerwingbox has an additional midspar to support the landing loads.
The simulation model is shown in figure 12. The number, positioning and orientation of the ribs were initially selected according to the specifications of the LR-270 configuration. The simulation model consists of linear shell elements with isotropic material behaviour. The mass distribution of engine, landing gear and fuel are considered as point masses and connected via rigid beam elements. The aerodynamic model is based on the linear potential theoretical double-lattice method (DLM) and contains the projected area of the airplane configuration.

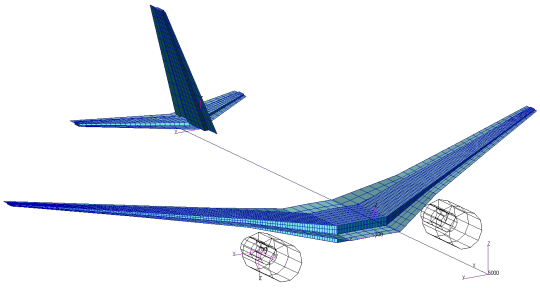

Fig. 12: LR-270 configuration.

Based on the resulting loads from the 2.5 g manoeuvre and the geometric and operational boundary conditions, the configuration is dimensioned using standardized procedures. The resulting parametric structural model is shown in the appendix in figure A.2 and forms the basis for further work on the design of the structure.

The middle and outer wing have a reduced wall thickness. The material thickness of the ribs is 4 mm and remains constant over the span. The wing box has a depth of 40% of the aerodynamic chord of the profile over the entire span of the wing and starts at 20% of the wing depth.

5.2.3 Influence of flap excitation

Based on the dimensioning loads of the reference configuration from chapter 5.2.1, the following section examines the influence of flap excitation. Hence, particularly loaded areas of the structure might be identified and can be taken into account in the design. The structure is mainly stressed due to manoeuvre and gust loads combined with the steady 1-g level flight. But due to the new flap concept different dynamic loads might additionally effect the structure.

The wingbox structure is given in figure 13. Therein the engine nacelle mass has been added rigidly by a concentrated mass of 8600 kg. The aerodynamic model has been extended for the simulation of transient flap excitation by separate trailing edge flaps as shown in figure 13. They can be excited with the required amplitude and frequency for the entire flight range. The lower frequency range is likely to be of interest for the increase in lift during the landing approach. The inboard flap is attached rigidly whereas the outboard flap is divided into an inner and outer part

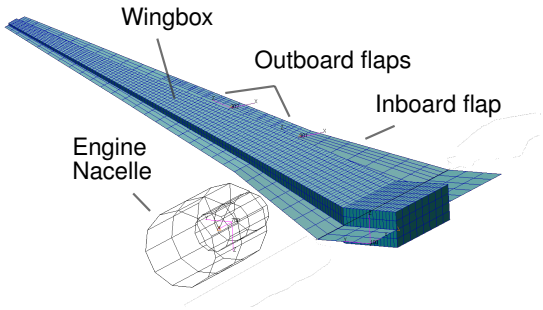

Fig. 13: Wing structure of the LR-270.

and have been inversely enforced by dynamic input during simulation.
The subsequent figures 14 and 15 show the deflection response of the wing tip and engine nacelle by the dynamic amplification factor (DAF). The DAF describes the ratio between dynamic structural response and the static response. As expected, the flap excites the entire structure including the engine nacelle.

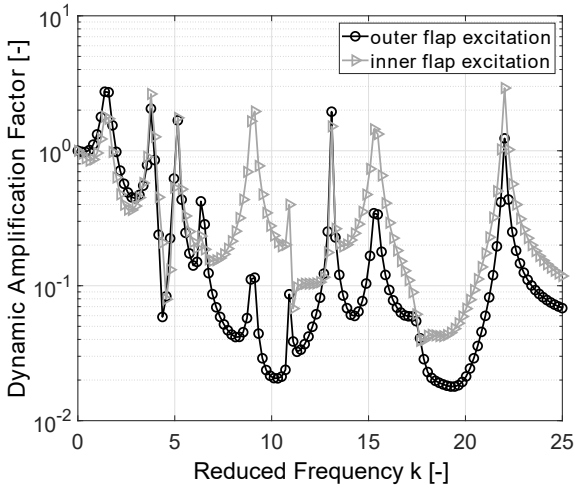

Fig. 14: DAF of wing tip displacement.

The plots are characterized by alternating resonance peaks and fields of off-peak response. The displacement response of the wing tip in the frequency range of interest is given in figure 14. The amplification of the structure depends mainly on the excited mode shape. Thus the outer flap excites primary the first bending mode of the structure at a reduced frequency of $k = 1.6$, due to the greater lever arm. The outboard flap close to the wing root excites mostly the higher mode shapes.

The main focus within this study is the lower frequency range.Therein the inner part of the flap excites particularly the engine nacelle, due to the sustained high peak at $k = 3.9$ as shown in figure 15. The strain energy plot given in figure 16 for harmonic flap excitation, indicates a high energy input at the frequency range between $3.5 \leq k \leq 5.3$. Therein the response is enforced by the inner as well as by the outer part of the flap.

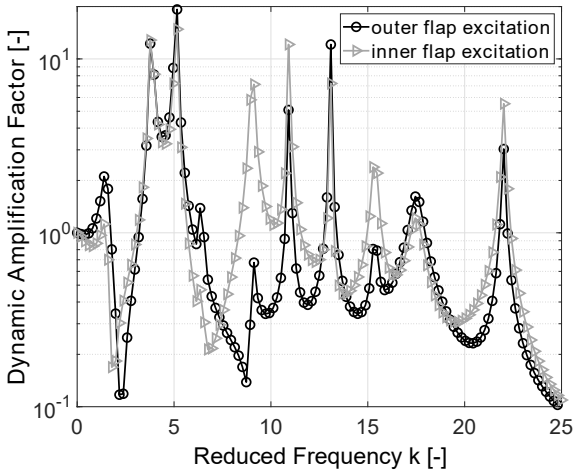

Fig. 15: DAF of engine nacelle displacement.

Taking into account the different definitions of the reduced frequencies from the equations 3 and 5, applied to the LR-270 the frequencies required for vortex instability excitation are below the critical structural response frequencies.

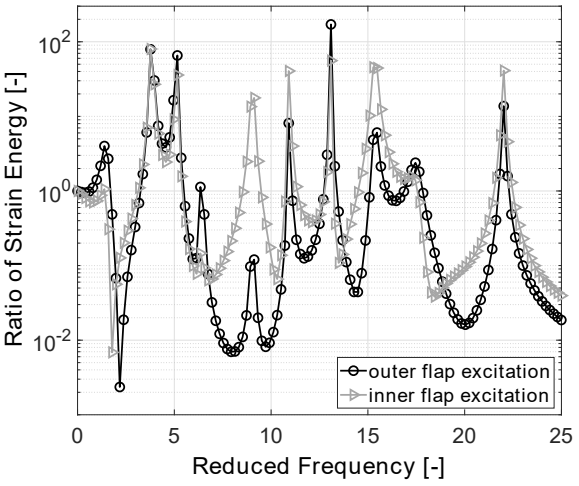

Fig. 16: Strainenergy due to outboard flap excitation.

In total, the strain energy input is greater than one in a wide frequency range. Therefore in the case of continuous flap excitation during landing approach the structure needs to be designed in more detail to take the dynamic enforcement into account. In addition, the flaps will be excited in inverse direction to compensate the lift change and thus the energy input will be further reduced.

6. CONCLUSION

This paper has shown the preliminary investigations of the vortex instability excitation and the high-lift augmentation by oscillating flaps. With the set up airplane configuration, a wind tunnel model for vortex instability investigations has been constructed and first results show that the induced frequency is propagated in the flow, which satisfies the necessary condition for excited vortex instabilities.
In regard of the lift coefficient, the gapless plain flap water tunnel model has shown only a lower effectiveness, thus configurations with a gap and other kinematics will be investigated further.
The high-lift system was described and the structural design has been conducted, which shows the effect of various reduced frequencies on the dynamic amplification factor and strain energy. The frequencies required for the vortex instability excitation are below the shown critical structural response frequencies.
Further studies regarding the vortex and lift alternation, as well as the actuation and structural detailed design will be conducted in the future.

ACKNOWLEDGEMENT

The funding of this investigation within the LUFO V3 project BIMOD (Influencing maximum lift and wake vortex instabilities by dynamic flap movement) (FKZ: 20E1702A) by the German Federal Ministry for Economic Affairs and Energy (BMWi), is gratefully acknowledged.

References

[1] ALBERTSON, J.; TROUTT, T.; SIURU, W.; WALKER, J.: Dynamic stall vortex development and the surface pressure field of a pitching airfoil. AIAA-87-Fluid Dynamics, Plasma Dynamics and Lasers Conference, 1987.

[2] ALLEN, A.: Beeinflussung des Nachlaufwirbelsystems von Transportflugzeugen. TU München, PhD thesis, 2009.

[3] ASHLEY, H.; VANECK, T.; JARRAH, M. A. M.; KATZ, J.: Unsteady aerodynamic loading of delta wings for low and high angles of attack, 1990.

[4] BILANIN, A. J.; DONALDSON, C. d.: Estimation of velocities and roll-up in aircraft vortex wakes. Journal of Aircraft, Vol. 12, No. 7, pp. 578–585, 1975.

[5] BILANIN, A. J.; TESKE, M. E.; WILLIAMSON, G.: Vortex interactions and decay in aircraft wakes. AIAA journal, Vol. 15, No. 2, pp. 250–260, 1977.

[6] CROW, S. C.: Stability theory for a pair of trailing vortices. In 8th Aerospace Sciences Meeting. American Institute of Aeronautics and Astronautics, 1970.

[7] CUI, E.; YU, X.; FU, G.; XU, C.; ZHANG, S.; ZHOU, M.: Separation Control and Lift Enhancement of Airfoil Using Unsteady Excitations. ICAS Proceedings, pp. 1208–1214, 1992.

[8] DONALDSON, C. d.; BILANIN, A. J.: Vortex Wakes of Conventional Aircraft, 1975.

[9] EICHLER, H.-J.; KRONFELDT, H.-D.; SAHM, J.: Das neue Physikalische Grundpraktikum: 3. Translation und Rotation. Ser. Springer-Lehrbuch, Berlin and Heidelberg: Springer Spektrum, 2016.

[10] EUROPEAN UNION AVIATION SAFETY AGENCY: Certification Specifications for Large Aeroplanes CS-25, ED Decision 2018/010/R.

[11] FEDERAL AVIATION ADMINISTRATION: Airworthiness standards: Transport category airplanes, FAA FARS, 14 CFR Part 25.

[12] GERZ, T.; HOLZÄPFEL, F.; DARRACQ, D.: Commercial aircraft wake vortices. Progress in Aerospace Sciences, Vol. 38, No. 3, pp. 181–208, 2002.

[13] GREENBLATT, D.; WYGNANSKI, I. J.: The control of flow separation by periodic excitation. Progress in Aerospace Sciences, Vol. 36, No. 7, pp. 487–545, 2000.

[14] GREENHALGH, S.: Oscillating Flap Lift Enhancement Device. Patent, 1999.

[15] HALLOCK, J. N.: Monitoring wake vortex strength decay near the ground. AIAA Journal of Aircraft, Vol. 13, No. 10, pp. 830–832, 1976.

[16] HARVEY, J. K.; PERRY, F. J.: Flowfield produced by trailing vortices in the vicinity of the ground. AIAA journal, Vol. 9, No. 8, pp. 1659–1660, 1971.

[17] HENKE, R.: Validation of wing technologies on an Airbus A340 flying testbed: First flight test results from the European program AWIATOR, 2004.

[18] HOEIJMAKERS, H. W. M.: Vortex Wakes in Aerodynamics. AGARD conference proceedings, No. 584, 1996.

[19] HOWE, D.: Aircraft conceptual design synthesis, London: Professional Engineering Publishing, 2010.

[20] HÜNECKE, K.: Structure of a Transport Aircraft-Type near Field Wake. AGARD conference proceedings, No. 584, 1996.

[21] HÜNECKE, K.: The characterisation of transport aircraft vortex wakes. AIAA Applied Aerodynamics Conference, 2001.

[22] IVERSEN, J. D.: Correlation of turbulent trailing vortex decay data. Journal of Aircraft, Vol. 13, No. 5, pp. 338–342, 1976.

[23] NELSON, R. C.; PELLETIER, A.: The unsteady aerodynamics of slender wings and aircraft undergoing large amplitude maneuvers. Progress in Aerospace Sciences, Vol. 39, No. 2-3, pp. 185–248, 2003.

[24] RAYMER, D.: Aircraft Design: A Conceptual Approach, Sixth Edition, Washington, DC: American Institute of Aeronautics and Astronautics, Inc, 2018.

[25] RECKZEH, D.: Multifunctional wing moveables: Design of the A350XWB and the way to future concepts. 29th Congress of the International Council of the Aeronautical Sciences, ICAS 2014, 2014.

[26] RECKZEH, D.: Aerodynamic design of the high-lift-wing for a Megaliner aircraft. Aerospace Science and Technology, Vol. 7, No. 2, pp. 107–119, 2003.

[27] RISSE, K.; ANTON, E.; LAMMERING, T.; FRANZ, K.; HOERNSCHEMEYER, R.: An Integrated Environment for Preliminary Aircraft Design and Optimization. In Structures, Structural Dynamics, and Materials and Co-located Conferences, 2012.

[28] ROSSOW, V. J.: Lift-generated vortex wakes of subsonic transport aircraft. Progress in Aerospace Sciences, Vol. 35, pp. 507–660, 1999.

[29] ROSSOW, V. J.: Prediction of span loading from measured wake-vortex structure-an inverse Betz method. Journal of Aircraft, Vol. 12, No. 7, pp. 626–628, 1975.

[30] RUDOLPH, P. K. C.: High-lift systems on commercial subsonic airliners, 1996.

[31] RUHLAND, J.; BREITSAMTER, C.: Numerical analysis of high-lift configurations with oscillating flaps: Deutsche Gesellschaft für Luft- und Raumfahrt - Lilienthal-Oberth e.V., submitted, 2019.

[32] SHEHATA, H.; ZAKARIA, M.; HUSSEIN, A.; HAJJ, M. R.: Aerodynamic Analysis of Flapped Airfoil at High Angles of Attack. In 2018 AIAA Aerospace Sciences Meeting.

[33] SPALART, P. R.: Airplane trailing vortices. Annual Review of Fluid Mechanics, Vol. 30, No. 1, pp. 107–138, 1998.

[34] STRÜBER, H.: The aerodynamic design of the A350 XWB-900 high lift system. 29th Congress of the International Council of the Aeronautical Sciences, 2014.

[35] TORENBEEK, E.: Synthesis of Subsonic Airplane Design, Dordrecht: Kluwer Academic Publishers, 1982.

[36] ZACCAI, D.; BERTELS, F.; VOS, R.: Design methodology for trailing-edge high-lift mechanisms. CEAS Aeronautical Journal, Vol. 7, No. 4, pp. 521–534, 2016.

APPENDIX

Fig. A.1: Airplane configuration LR-270 built with MICADO.

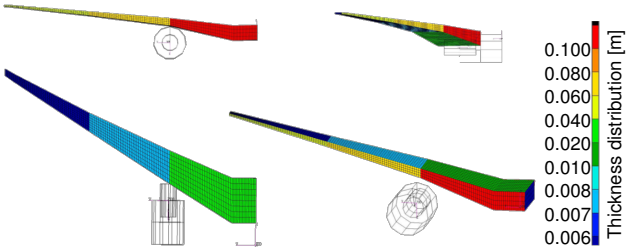

Fig. A.2: Thickness distribution of the LR-270 configuration structural model.

Parameter	
Cross section of test section	1.80 m x 2.40 m
Length of the test section	4.80 m
Maximum speed	65 m/s
Turbulence level	$Tu_x = Tu_y = Tu_z < 0.4\%$
Test section	open

Tab. 7: Specifications of wind tunnel A (closed return).

Parameter	
Cross section of test section	1.80 m x 2.70 m
Length of the test section	21.00 m
Maximum speed	30 m/s
Turbulence level	$Tu_x = Tu_y = Tu_z < 0.5\%$
Test section	closed

Tab. 8: Specifications of wind tunnel C (closed return).